AIP | Journal of Applied Physics

Mechanisms of nanodot formation under focused ion beam irradiation in compound semiconductors

K. A. Grossklaus and J. M. Millunchick

Citation: J. Appl. Phys. **109**, 014319 (2011); doi: 10.1063/1.3530839
View online: http://dx.doi.org/10.1063/1.3530839
View Table of Contents: http://jap.aip.org/resource/1/JAPIAU/v109/i1
Published by the AIP Publishing LLC.

Mechanisms of nanodot formation under focused ion beam irradiation in compound semiconductors

K. A. Grossklaus[a] and J. M. Millunchick[b]
Department of Materials Science and Engineering, University of Michigan, Ann Arbor, Michigan 48109-2136, USA

(Received 6 July 2010; accepted 18 November 2010; published online 13 January 2011)

We have examined the responses of GaAs, InP, InAs, and AlAs to 30 keV focused ion beam (FIB) irradiation and applied a unified model that consistently explains the observed effects. Nanodots were observed to form on GaAs, InP, and InAs under irradiation at normal incidence, while nanodots are not observed on AlAs. The FIB response and nanodot formation behavior of each material is discussed with regard to a few basic material properties and a model for nanodot creation and growth by the action of preferential sputtering and Ostwald ripening. The model predicts the development of a stable average nanodot size with increasing ion dose, with the average nanodot size depending on the excess group III adatom yield, adatom surface diffusion rate, and surface tension. These predictions qualitatively agree with the experimentally observed trends for GaAs and InP. They also agree for the initial nanodot formation on InAs, but this material system exhibits a sudden transition in the nanodot size distribution. The model predicts that nanodots will have difficulty forming and growing on AlAs, which is also in agreement with our experimental results.
 [doi:10.1063/1.3530839]

I. INTRODUCTION

The self-assembly of group III metallic nanodots and other nanostructures of the III-V compound semiconductors has recently become a topic of much interest. For instance, group III metallic nanodots and clusters show interesting optical qualities[1,2] that make them promising for use in negative index of refraction materials. They also have application in the creation of quantum dots by droplet epitaxy[3–5] and in nanowire growth.[6] While it is possible to create group III dots by direct deposition of metal atoms on a surface,[3–5] it is also possible to induce their formation in compound semiconductors using ion irradiation.[7–10] Both of these methods provide a simple synthesis route for the creation of nanostructures over large areas, but a drawback is that those nanostructures may be at random locations and in a distribution of sizes. Focused ion beam (FIB) irradiation of III-V compound semiconductors has shown promise as a viable approach for producing nanoscale group III metallic nanodots at random locations,[7–10] in self assembled arrays,[11] and at selected locations via patterning.[11–13] As such, FIB irradiation serves as both a bottom-up and top-down method for the creation of nanostructures on semiconductor surfaces. In order for FIB created metallic nanostructures to be used reliably in device applications, the physical mechanisms and processing parameters that govern their creation need to be understood.

The metallic nanostructures that develop on a semiconductor surface depend strongly on the material being irradiated, and a series of previous studies have individually shown that each III-V compound responds differently to FIB irradiation. The Ga^+ FIB response of GaAs,[7,10,11,14,15] InP,[13] InAs,[8] and GaSb (Refs. 16 and 17) substrates have all been examined. FIB irradiation of InP, GaAs, and InAs in those studies has been shown to produce group III nanodots of varying sizes and morphologies, a phenomenon which has been attributed to preferential sputtering of the group V element followed by assembly of the excess group III atoms.[7–9,11,12] The FIB-created metallic nanodots on GaAs and InAs have been identified as nearly pure Ga (Refs. 11, 14, and 15) and In (Ref. 8), respectively. Previous FIB studies of InP do not identify the composition of the nanodots in that system.[13] However, other studies examining low energy inert gas ion irradiation of InP have identified the nanodots as In-enriched.[18–20] Nanostructure creation on irradiated GaSb has been shown to produce cellular voids, a network of stoichiometric nanoscale GaSb wires, and Ga precipitates on those wires depending on ion dose,[16,17] all of which are presumed to form due to the movement and coalescence of ion-damage created point-defects.[21,22]

Regardless of intended application and nanostructure placement requirements, if a FIB method is to be used to create reproducible and useful nanostructures, the FIB responses of the III-V semiconductors as a material system need to be carefully measured and theoretically understood. Previous studies of the FIB response of III-V binary compounds have focused on the response of each III-V compound individually, and except for the case of GaAs,[11,14] have not carefully tracked the development of nanostructure sizes on each compound as a function of increasing ion dose. A coherent physical picture of how ion induced nanodot formation proceeds that spans material systems is still lacking. If strategies for FIB induced creation of nanostructures for a variety of applications are to be developed, then a compari-

[a]Electronic mail: kgrosskl@umich.edu.
[b]Electronic mail: joannamm@umich.edu.

son of FIB response across multiple materials is needed that relates their response to fundamental mechanisms driving nanostructure creation.

This study examines the 30 keV Ga^+ FIB response of GaAs, InAs, InP, and AlAs and the distribution of metallic nanodots formed on each material as a function of increasing 30 keV Ga^+ FIB dose in order to compare the different responses of those materials based on a few basic physical properties. Careful tracking of nanodot development as a function of ion dose has not been reported for InAs, InP, or AlAs, and a comparison across this set of materials has not been previously conducted. The FIB response of each material is characterized by ion-induced secondary electron (ISE) microscopy or scanning electron microscopy (SEM), x-ray energy dispersive spectroscopy (EDS), and atomic force microscopy (AFM). Based upon these experimental observations, we employ a simple model that incorporates basic physical drivers for nanodot creation in order to provide a description of how they affect the FIB response of each compound semiconductor. No similar study comparing and attempting to explain the different nanodot forming behavior of multiple III-V materials in terms of the material properties and physical processes common to all has previously been reported in the literature. The nanoscale wire forming FIB response of GaSb, while remarkable, does not lend itself to direct comparison with the metallic nanodot forming response of the other materials as it is driven by a fundamentally different mechanism. Thus the theory developed in this work does not attempt to incorporate the response of GaSb.

II. EXPERIMENTAL DETAILS

The FIB responses of GaAs, InP, and InAs (001) substrates were determined by irradiating each with a Ga^+ FIB and characterizing the results. All wafers were commercially obtained epi-ready substrates intended for use in epitaxial film growth. Analysis of the response of those materials to ion irradiation was conducted using a FEI Nova Nanolab dual-beam FIB system equipped with a field-emission scanning electron microscope and a FEI Magnum ion column capable of producing a 5–30 keV Ga^+ beam. An ion beam energy of 30 keV was used for all experiments, while beam current and applied dose were varied.

The FIB response of AlAs films grown on GaAs (001) wafers was also examined. In order to avoid oxidation of the AlAs between the time of growth and FIB exposure, a FEI UHV Magnum ion column connected *in vacuo* to an EPI 930 MBE growth system was used for these studies. Approximately 50 nm thick AlAs films were grown on GaAs at a temperature of 620 °C and at a rate of approximately 0.5 ML/s in the MBE system and then transferred to a separate vacuum chamber containing the ion column. As in the case of the other materials examined, the energy of the ion beam used to examine the AlAs films was maintained at 30 keV while beam current and dose were varied.

In order to examine the FIB response of these III-V materials, square regions ranging in size from 1 to 100 μm^2 were irradiated. The ion beam was repeatedly scanned in a serpentine pattern over each sample area in order to achieve the desired ion dose. A beam spot overlap of 50% and a dwell time of 1 μs at each spot were used in all cases. Beam dwell time was maintained at 1 μs, as changing dwell time was observed to have an effect on the final distribution of nanodots in some cases. During irradiation, the ion beam was kept at normal incidence to the substrate. FIB irradiation was carried out using beam currents ranging from 5 to 290 pA and ion doses ranging from 10^{15} to 10^{18} ions/cm^2. By irradiating different areas with varying doses it was possible to examine the tendency of each material to form metallic nanodots, determine the ion dose at which nanodots first appear, examine the development and size distribution of those structures with increasing ion dose, and establish the FIB milling rate of each material.

Following irradiation, characterization of each material was carried out using several techniques. GaAs, InP, and InAs samples were examined *in situ* in the Nova dual-beam FIB system by SEM immediately before and following ion irradiation. In the cases where nanodots formed their size and distribution were characterized immediately following formation by SEM and their composition was probed using an attached EDS system. EDS was used to verify that the primary constituent of the nanodots was the group III element corresponding to the III-V compound they were produced on. SEM examination of areas irradiated with different ion doses was also used to identify the threshold dose for group III nanodot formation. Average nanodot sizes and distributions for each dose were found through image analysis of SEM micrographs and plotted to allow examination of trends in nanodot size as a function of ion dose. For consistency's sake and to allow examination of metallic nanodots away from any effect of the pattern edge, images for nanodot size analysis were taken only from large 10×10 μm square regions irradiated using a 0.3 nA FIB aperture, with actual measured beam currents ranging from 0.28 to 0.29 nA. Immediately following removal from the dual-beam FIB system, samples were examined using a Nanoscope IIIa AFM to corroborate nanodot sizes, measure ion milling depths in the irradiated regions of GaAs, InP, and InAs samples, and verify the threshold dose for nanodot formation determined by SEM. Milling depth measurements did not take into account the effect of ion-induced swelling. The AlAs films grown on GaAs were examined *in situ* by ISE, with a resolution limit of approximately 20 nm due to vibration of the vacuum system. Beyond limited ISE imaging it was not possible to characterize the AlAs films without first removing those films from vacuum. Upon removal from vacuum they were taken and characterized as quickly as possible by AFM in a manner similar to the other III-V materials. However, upon exposure to atmosphere the AlAs films began to visibly oxidize within a few minutes. Following AFM evaluation AlAs films were also placed into the dual-beam FIB system and characterized by SEM and EDS.

III. RESULTS

In agreement with work of previous authors,[7,8,10,11,13–15] metallic nanodots were observed to form on GaAs, InP, and InAs wafer substrates following 30 keV Ga^+ FIB irradiation. No resolvable nanodots were observed by ISE examination

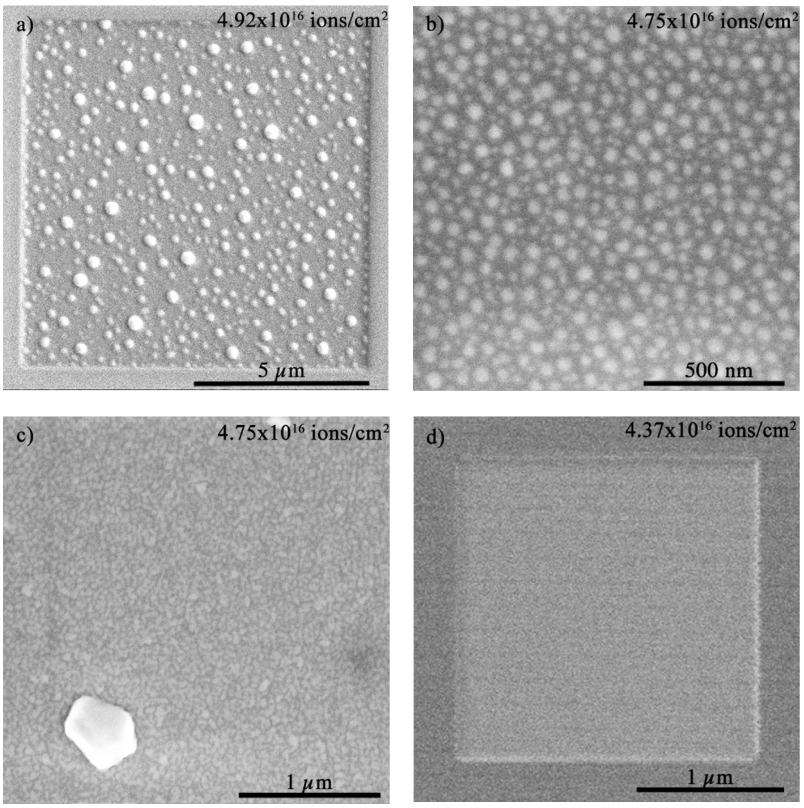

FIG. 1. Four electron micrographs comparing areas of (a) GaAs, (b) InP, (c) InAs, and (d) AlAs following FIB irradiation with similar ion doses. Ion dose is indicated in the upper right corner of each image. Please note the different scale bars sizes for each image.

in vacuo or by later *ex situ* AFM examination of the AlAs films following irradiation, even up to the maximum applied dose of $>6.24\times10^{16}$ ion/cm^2, past which the AlAs films were completely milled through. The different responses of GaAs, InP, InAs, and AlAs are demonstrated in Fig. 1, which shows an area of each material following exposure to similar ion doses of approximately 4×10^{16} to 5×10^{16} cm^{-2}. As can be seen from the figure, GaAs, InP, and InAs form nanodots with different average sizes and size distributions at comparable ion dose. Table I shows various FIB response values for each material: r, the experimentally determined milling rate, D_{max}, the maximum dose before the initial appearance of nanodots, and h_{max}, the maximum depth that can be milled to before the appearance of nanodots, calculated using the values of r and D_{max}. Milling rates were determined by using AFM to measure the depths relative to the undisturbed wafer surface milled to by different ion doses. The maximum dose before initial nanodot formation was determined by milling 5×5 and 2×2 μm squares at increasing doses and noting the point at which nanodots were first observed by SEM and AFM. This approach is then inherently limited by the minimum nanodot size capable of being resolved by the SEM and AFM instruments used, and it is possible that metallic nanodots smaller than the clearly resolvable size formed at lower doses. The resolution of the SEM and AFM systems used to image all four materials was limited to ~5 nm, while the ISE imaging system used to initially examine the AlAs films *in vacuo* was limited to ~20 nm. Comparing the r and D_{max} values given in Table I, it can be seen that InP and InAs both mill quickly and produce droplets at relatively low doses. AlAs has a significantly lower FIB milling rate than any of the other three materials studied and does not produce droplets. The lower milling rate of AlAs is not unexpected, as AlAs has been previously shown to be more resistant to ion damage than the other III-V compounds.[23,24]

TABLE I. Comparison of the experimentally found milling rate, r, the maximum FIB dose before nanodot appearance, D_{max}, and the maximum depth that can be milled to before the appearance of nanodots, h_{max}, for each of the III-V materials studied. ± values represent 1 standard deviation from the mean plus AFM measurement error.

	r (μm^3/nC)	D_{max} (ions/cm^2)	h_{max} (nm)
GaAs	0.77 ± 0.12	1.7×10^{16}	21
InP	1.07 ± 0.11	1.7×10^{15}	3
InAs	1.25 ± 0.15	6.4×10^{15}	13
AlAs	0.36 ± 0.06	N/A	N/A

In addition to the milling rate and dose at which group III metallic nanodots first appear, the manner with which the distributions of nanodots in the FIB irradiated regions develop also differs for GaAs, InP, and InAs. Following their initial appearance, Ga nanodots on GaAs grow to a stable average size over a dose range of 1×10^{16} to 1×10^{17} ions/cm^2. Figure 2(a) shows the evolution of nanodot size as a function of ion dose, while Figs. 2(b)–2(d) show SEM images taken of the GaAs nanodot distribution at increasing ion doses which are indicated on Fig. 2(a). Nanodots on GaAs reach a stable average nanodot size of approximately 150 ± 10 nm with a broad distribution of sizes.

Nanodots on InP grow over a shorter dose interval of approximately 1×10^{15} to 2×10^{16} ions/cm^2 to a smaller stable average diameter of approximately 33 ± 3 nm and into a stable distribution of sizes. Figure 3(a) shows the evo-

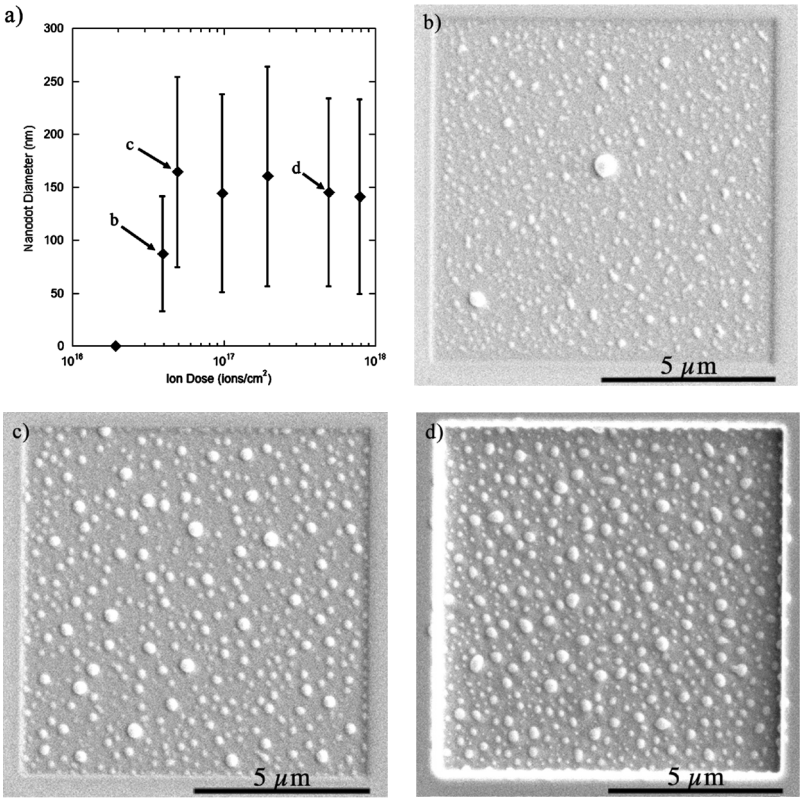

FIG. 2. A plot and SEM images showing change in nanodot size as a function of dose in FIB irradiated regions of GaAs. (a) shows average nanodot diameter plotted as a function of dose, with error bars indicating nanodot diameters up to one standard deviation above and below the mean for each value. (b), (c), and (d) show images at the doses corresponding to the matching points indicated in (a).

lution of nanodot size on InP as a function of ion dose, and Figs. 3(b)–3(d) show SEM images taken of the InP nanodot distribution at increasing doses indicated in Fig. 3(a). Barring the differences in doses and sizes, the nanodot versus dose trends exhibited by InP and GaAs are similar, with both materials reaching a stable average nanodot size and distribution after a short initial growth period.

Fig. 4(a) shows the evolution of nanodots on InAs as a function of ion dose and Figs. 4(b)–4(d) show SEM images taken of the InAs nanodot distribution at increasing doses. InAs shows an initial period of nanodot growth above its threshold dose and begins to approach a stable distribution in a manner similar to InP and GaAs. However, rather than reaching a stable average size and distribution, the nanodot

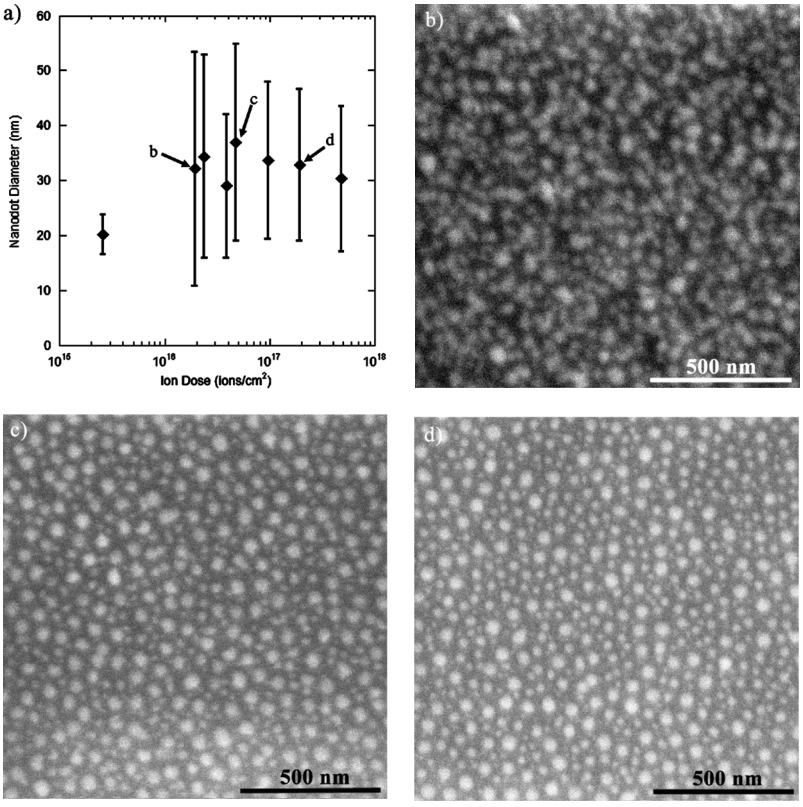

FIG. 3. A plot and SEM images showing change in nanodot size as a function of dose in FIB irradiated regions of InP. (a) shows average nanodot diameter plotted as a function of dose, with error bars indicating nanodot diameters up to one standard deviation above and below the mean for each value. (b), (c), and (d) show images at the doses corresponding to the matching points indicated in (a).

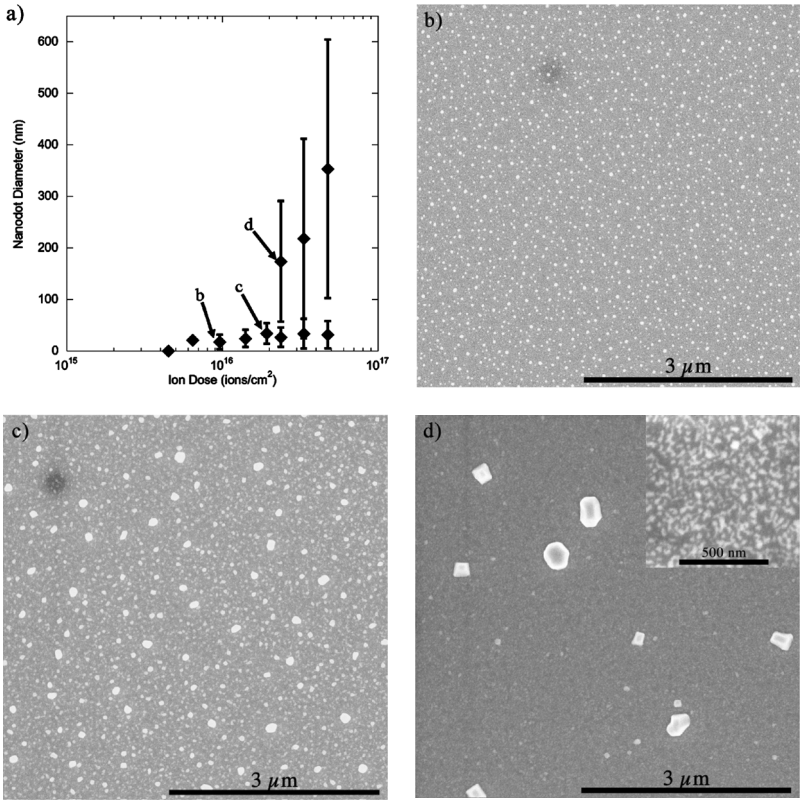

FIG. 4. A plot and SEM images showing change in nanodot size as a function of dose in FIB irradiated regions of InAs. (a) shows average nanodot diameter plotted as a function of dose, with error bars indicating nanodot diameters up to one standard deviation above and below the mean for each value. Above ~2e16 ions/cm^2 the data diverges into two sets of data which indicate the bimodal nature of the nanodot size distribution. (b), (c), and (d) show images at the doses corresponding to the matching points indicated in (a). The inset image in (d) shows the small nanodots that occupy all the irradiated area surrounding the very large nanodots in (d).

size distribution of InAs abruptly becomes bimodal at a dose of approximately 1.9×10^{16} ions/cm^2. This sudden change is shown in Fig. 4(a) by a splitting of the nanodot size data into larger and smaller nanodot distributions above a dose of 1.9×10^{16} ions/cm^2 and by the rapid increase in the size of In nanodots/particles visible in the larger particle data set. This change can also be seen by noting the significant change in nanodot size distribution between the images shown in Figs. 4(c) and 4(d). The large In particles reach sizes greater than 600 nm and exhibit clear faceting. This transition and faceting of large nanodots on InAs is evident in the experiments of Lugstein *et al.* as well,[8] though it is not noted as a sharp, repeatable transition by those authors. No nanodot faceting was observed in the case of the GaAs or InP. By comparing the drastic differences in group III metallic nanodot size, shape, and distribution for GaAs, InP, and InAs visible in Figs. 2–4, respectively, the very different FIB responses of these materials are made readily apparent.

IV. DISCUSSION

Despite the commonalities in the crystalline structures of GaAs, InP, InAs, and AlAs, the results presented above highlight the different FIB response and nanodot forming behavior of each material. A broader understanding of the FIB response of these materials is required for FIB directed tailoring of nanostructures to be used for demanding electronic and optoelectronic applications. The formation of metallic nanodots on III-V semiconductors under ion irradiation has been attributed to the preferential sputtering of the group V element,[9,19,25] followed by nucleation, growth and ripening of group III nanodots.[15] It is reasonable then to assume that the material properties that determine the FIB response of the III-V materials studied here are those that have a strong effect on their multicomponent sputtering behavior and the ability of free group III atoms to diffuse on the surface, nucleate into metallic nanodots, and grow into a distribution of nanodot sizes.

Following the theoretical work of Sigmund concerning preferential sputtering in a multicomponent system,[26] the properties that affect the relative partial sputtering yields of the group III and group V atoms, Y_{III} and Y_V respectively, are elemental surface binding energy and atomic mass. Here the sputtering yield is defined as the number of atoms sputtered per incident ion. The ratio of Y_{III} to Y_V in the linear cascade regime is approximated by:

$$\frac{Y_{III}}{Y_V} = \frac{c_{III}}{c_V}\left(\frac{M_V}{M_{III}}\right)^{2m}\left(\frac{U_V}{U_{III}}\right)^{1-2m}, \quad (1)$$

where c_{III} and c_V are atomic concentrations at the material surface, U_{III} and U_V are the surface binding energies of each element, and M_{III} and M_V are the atomic masses of the group III and group V species, respectively. m is the sputtering exponential factor, which is dependent on the reduced energy, ε, for each atom-ion pair and E, the energy of each incident ion. In developing Eq. (1), Sigmund makes the assumption that the compound being sputtered is amorphous and homogeneous. Previous work with Si^+ implantation of GaAs, InP, and InAs has shown that at ion doses of ~1 $\times10^{15}$ ions/cm^2 the near surface region of these materials is amorphized by ion damage,[23,24] indicating that the assumption of an amorphous medium in this study is reasonable. Those same studies demonstrated that AlAs is much more resistant to amorphization and remains crystalline to much higher doses. An m value may be defined for each atomic

TABLE II. Approximated group III and V surface binding energies used for sputter yield ratio calculations, U_{III} and U_V respectively, the group III surface enrichment predicted by Eq. (2), c^s_{III}/c^s_V, and the partial sputter yield ratio calculated using Eq. (1), Y_{III}/Y_V. The surface binding energies given for Ga, In, Al, and As are elemental heats of sublimation taken from Ref. 29. The value given for P is its elemental heat of formation from a gas taken from Ref. 30.

	U_{III} (eV/atom)	U_V (eV/atom)	c^s_{III}/c^s_V	Y_{III}/Y_V
GaAs	2.82	1.26	1.68	0.60
InP	2.49	3.28	1.28	0.78
InAs	2.49	1.26	1.82	0.55
AlAs	3.38	1.26	1.39	0.72

species, but component specific m values are not readily available in the literature. Therefore, a single m value is used in this work, a condition most valid when $M_V \approx M_{III}$.[26] For sputtering applications, m takes a value between $0 \leq m \leq 0.2$.[27] Malherbe *et al.* found a value of $m=0.165$ to be consistent with their results for Ar^+ ion sputtering of (100) InP surfaces[28] and this is the value we adopt here.

Atomic surface binding energies are often approximated as the elemental heat of sublimation or heat of formation from gaseous atoms, which when used in Eq. (1) produces reasonable results for metallic alloys.[26,27] The strong nonmetallic bonding in the III-V compounds will have a large impact on their surface binding energies, making the use of elemental heats of sublimation less accurate in predicting their behavior. However, experimental values for the surface binding energies of the III-V atomic constituents are not readily available, so we use the elemental heats of sublimation/formation (Table II).[29,30] Based solely on those values it would be expected that upon sputtering the surfaces of GaAs, InAs, and AlAs would become group III enriched, as in their cases $U_{III} > U_V$. This is in agreement with experimental observations for GaAs and InAs. Based on the magnitude of the Al and As binding energies the surface of AlAs is expected to become group III enriched upon irradiation, but metallic nanodots were not observed here. For the case of InP $U_{III} < U_V$, indicating that based on heat of sublimation alone its surface would be expected to become group V enriched. This is not the case, as nanodots have been experimentally observed on InP in this study and previous inert gas sputtering studies have identified them as comprised of In.[18–20] The cases of InP and AlAs demonstrate that the surface binding energy alone is insufficient to predict the sputtering response of these compound materials and that more complex relationships must be used to understand their observed behavior.

Another term that needs consideration is the ratio of the elemental surface concentration during sputtering, c_{III}/c_V, but its determination is nontrivial. At the start of sputtering c_{III}/c_V has a value of 1, the ratio of the elemental concentrations in the bulk. As sputtering proceeds the action of preferential sputtering will enrich the surface with the more slowly sputtering element, and in response the partial sputtering yield of that element will increase. In the absence of other competing effects, a steady-state will be achieved when the partial sputtering yield of the enriching element has increased to the point where it equals the sputtering yield of the other element. At this point the partial sputtering yield ratio, Y_{III}/Y_V, will reach a constant value of 1 and the elemental surface concentration ratio will have reached a constant maximum steady-state value. Using the form for the partial sputtering yields given in Eq. (1), the enrichment of the surface at steady-state, c^s_{III}/c^s_V, may be predicted by[26]

$$\frac{c^s_{III}}{c^s_V} = \frac{c^b_{III}}{c^b_V}\left[\left(\frac{M_V}{M_{III}}\right)^{2m}\left(\frac{U_V}{U_{III}}\right)^{1-2m}\right]^{-1}, \tag{2}$$

where c^b_{III} and c^b_V are the bulk concentrations of the group III and group V elements, respectively. Values for c^s_{III}/c^s_V predicted using Eq. (2), $m=0.165$, and the elemental heats of fusion, range in value from 1.2 to 1.9 (Table II). This approach does not take the nucleation of nanodots into account, which would deplete the surface of group III atoms. Thus, growth of nanodots will decrease the final level of group III surface enrichment and may also prevent the steady-state case of $Y_{III}/Y_V = c^b_{III}/c^b_V$ from ever being achieved. The result of Eq. (2) may serve as a theoretical upper limit for group III surface enrichment such that from the start of sputtering the surface concentration ratio will vary within the bounds of $c^b_{III}/c^b_V \leq c_{III}/c_V < c^s_{III}/c^s_V$. There will also be a significant Ga concentration in the near surface region due to implantation from the FIB, which for the case of GaAs will affect the relevant group III surface concentration. The fraction of Ga ions that remain on the surface at steady state, ζ, can be predicted by the method given in Ref. 31 and using Y_{III}/Y_V and c^s_{III}/c^s_V. This value has been taken here as $\zeta=0.1$.[11,32] However, as the Ga ions from the FIB are a different group III species than that present in InP, InAs, and AlAs, the contribution of Ga to the surface composition will be neglected except for in the case of GaAs.

A prediction of Y_{III}/Y_V found using Eq. (1) with the elemental heats of sublimation, $m=0.165$, and $c_{III}/c_V = c^b_{III}/c^b_V = 1$ is tabulated in Table II. Examining the zero fluence case, where $c_{III}/c_V = 1$, will provide Y_{III}/Y_V values that are representative of each III-V compound and can be used to compare their behavior. From Table II it can be seen that Eq. (1) predicts a Y_{III}/Y_V value less than 1 for all four III-V compounds studied, indicating preferential sputtering of the group V element will occur and result in an excess of the group III element. An approximate yield of excess group III atoms per incident ion can then be calculated using the total sputter yield for each compound. The total ion sputter yields, $Y_{total} = Y_{III} + Y_V$, have been approximated by multiplying the experimental milling rate values listed in Table I by the bulk atomic volume of each compound and are listed in Table III. The number of excess group III atoms generated per ion, Y_E, may be estimated using the experimental Y_{total} value, the zero fluence Y_{III}/Y_V ratio predicted by Eq. (1), and the relationship

$$Y_E = Y_{total}\left[\frac{1}{(Y_{III}/Y_V + 1)} - \frac{1}{(Y_V/Y_{III} + 1)}\right]. \tag{3}$$

The calculated values of Y_E for each compound are given in Table III. It should be noted that several simplifications have

TABLE III. The partial sputter yield ratios calculated using Eq. (1), Y_{III}/Y_V, the approximate total III-V sputter yield, Y_{total}, calculated using the experimental r values listed in Table I, and the estimated excess group III adatom yields, Y_E, calculated using Y_{total} and the results of applying Eqs. (1) and (3).

	Y_{III}/Y_V	Y_{total} (atoms/ion)	Y_E (excess group III atoms/ion)
GaAs	0.60	5.5	1.48
InP	0.78	6.8	0.83
InAs	0.55	7.2	2.09
AlAs	0.72	2.5	0.41

been made in calculating the Y_E values, therefore they should be treated with caution. It is best to use the values of Y_E only to compare the behaviors of each compound relative to one another and provide some insight into the nature of their FIB responses. For the case of GaAs, the number of excess Ga atoms will be increased by $\zeta=0.1$, the fraction of Ga^+ ions directly from the FIB beam that remain on the surface at steady state. In order to take this into account, the GaAs Y_E value given in Table III was found by taking the sum of ζ and the Y_E value predicted by Eq. (3).

Comparing the Y_{III}/Y_V and Y_E values given in Table III, it can be seen that preferential sputtering of the group V element and production of excess group III atoms on the material surface is expected for each of the four III-V compounds studied here. Materials with high Y_{III}/Y_V ratios and low Y_{total} values such as InP and AlAs have lower predicted Y_E values. However, a low Y_E value only indicates that enrichment of the surface with group III atoms before nanodot nucleation and nanodot growth after nucleation will be slow, and does not preclude nanodot formation or nanodot growth to larger sizes.

To develop further a satisfactory explanation for the different FIB responses of GaAs, InP, InAs, and AlAs a model must be employed that describes the transport of group III atoms across their respective irradiated III-V surfaces and how transport and excess group III production compete with sputtering losses to determine metallic nanodot growth and size distribution. A suitable model has been developed by Wei, *et al.*[11,32] in order to describe their results for off-normal FIB bombardment of GaAs. Their approach was to modify the classic model for Ostwald ripening in a diffusion-limited system[33] to accommodate the effects of sputtering from and implantation into Ga nanodots by a FIB and continuous generation of excess group III atoms on the III-V surface. They arrive at the their final model through the solution of the diffusion equation in polar coordinates, with an additional source term to account for the generation of excess Ga adatoms from preferential sputtering and with each nanodot assumed to be a hemispherical cap surrounded by a denuded adatom capture zone. We adopt the general approach of Wei *et al.* with some slight modifications to generalize it for other compounds and to incorporate the form of Y_E developed above, again assuming diffusion rather than interface attachment limited behavior. The detailed development of the model as adapted for this study is given in the appendix, and follows closely the derivation of Wei *et al.*[32] The evolution of the nanodot radius of curvature, R, as a function of time, t, is given by

$$\frac{dR}{dt} = A\left(1 - \frac{R^*}{R} + BR^2\right), \tag{4}$$

where

$$A(R) = \frac{D_{III}(C_\lambda - C_0)\Omega_{III}}{R^2 \ln(\lambda/R)},$$

$$R^* = \frac{2\Omega_{III}\gamma C_0}{kT(C_\lambda - C_0)},$$

$$B(R) = \left(\frac{Y_E I \ln(\lambda/R)}{2D_{III}(C_\lambda - C_0)}\right)\left[\frac{(\lambda/R)^2 - 1}{\ln(\lambda/R)^2} - 1 - 2\left(\frac{Y^*_{III}\Omega_{III} - 0.5\Omega_{Ga}}{Y_E\Omega_{III}}\right)\right]. \tag{5}$$

D_{III} is the coefficient of ion enhanced diffusion for group III atoms on an irradiated III-V surface, Ω_{III} is the atomic volume of the group III element, λ is the nanodot denuded zone radius past which the adatom density recovers its average value, C_λ is the adatom concentration at λ, C_0 is the flat-surface equilibrium group III adatom concentration, γ is the metallic nanodot-vapor surface tension, k is the Boltzmann constant, T is the absolute temperature, I is the flux of incoming ions, Y^*_{III} is the sputtering yield of the pure group III element taken to approximate the sputtering yield from a nanodot, and Ω_{Ga} is the atomic volume of a gallium. As defined in Eq. (4), R^* is the critical nanodot size and B is the sputtering dependent parameter. A is a positive term and represents the contribution of Ostwald ripening, such that when $B=0$ Eq. (4) reduces to the standard equation for diffusion limited Ostwald ripening in a conservative system.[34] For the case of sputtering from the nanodot, B will have a value less than zero.

As a result of $B<0$, Eq. (4) predicts that once the average nanodot size reaches a critical value the competing effects of atoms being sputtering from the nanodot, ions being implanted into it, and adatoms diffusing to it will balance each other and produce a stable average nanodot size. Wei *et al.* used this result to explain the creation of a stable array of uniform and stationary Ga nanodots with off-normal FIB bombardment of GaAs.[11] Because in this study the FIB was at normal incidence, new nanodot nucleation, growth, and coalescence with other dots was continual, preventing the creation of a single uniform nanodot size. Despite this, the experimental results presented above show that a stable distribution of nanodot sizes will develop for normal incidence FIB irradiation of GaAs and InP in agreement with the prediction of Eq. (4), and InAs begins to develop a stable distribution before it is prevented from doing so by its nanodot size transition.

The property dependencies and general trends described by Eqs. (4) and (5) can be used to describe the behavior of the III-V systems. Because many of the property values required by Eq. (5) are not readily available or only available

TABLE IV. A list of group III metal properties which play a part in determining the nanodot forming behavior of the III-V compounds. Tabulated are the metal-vapor surface tension, γ, the homologous melting temperature at 300 K, T_H, SRIM-2008 predicted elemental sputter yield, Y^*_{III}, and atomic volume, Ω_{III}, of each group III metal examined in this work.

	γ (J/m^2)	T_H at 300 K	SRIM-2008 Y^*_{III} (atoms/ion)	Ω_{III} (m^3/atom)
Ga	0.767	0.990	6.1	1.96×10^{-29}
In	0.633	0.698	11.2	2.61×10^{-29}
Al	1.14	0.321	3.9	1.65×10^{-29}

by approximation, Eqs. (4) and (5) are not suitable for quantitatively predicting average nanodot sizes and distributions relative to the results reported here. The trends of Eqs. (4) and (5) indicate that higher values of D_{III} and Y_E will, respectively, result in a higher rate of growth by Ostwald ripening, indicated by the coefficient A, and a less negative value of B. Both effects will result in sputtering losses taking longer to balance nanodot growth and so result in a larger stable average nanodot size. Conversely, higher values of Y^*_{III} and γ will make B more negative and lower R^*, resulting in a smaller final nanodot size. A high γ value is also indicative of a high barrier for nanodot nucleation and so will affect the point at which nanodots are initially able to form. Nanodot size is influenced by all four of the above quantities, and they will be used as a basis for explaining the relative differences in nanodots size for the four materials studied.

In order to facilitate a comparison across the materials studied, some of the physical quantities specified in Eq. (5) for the group III metals are listed in Table IV. γ values were taken from Ref. 35 and are the surface tension of the solid group III metal species for each III-V compound. Y^*_{III} values were calculated using 10 000 ion SRIM-2008 (version 2008.05) (Ref. 36) simulations of 30 kV Ga^+ implantation into an amorphous solid of each respective group III atom.[37] Ω_{III} values were approximated by converting to the appropriate units from the room temperature density and molar mass of each solid metallic element. The homologous melting temperature at 300 K, $T_H=300/T_M$, of each group III metal is listed in place of a D_{III} value, with melting temperatures, T_M, taken from Ref. 29. T_H is assumed to be an indicator of the relative magnitude of D_{III}, with higher values of T_H indicating that the group III element is nearer to its bulk melting temperature and can be expected to diffuse more rapidly across the III-V surface.

Through the use of Eqs. (4) and (5) and the properties given in Tables III and IV, a number of trends may be predicted that reflect experimental observations. Equation (4) predicts that a balance will develop between nanodot volume loss to sputtering and nanodot growth by diffusion of adatoms and implantation of Ga ions. The development of stable average nanodot sizes and distributions after prolonged irradiation of GaAs (Fig. 2) and InP (Fig. 3) may be explained on the basis of this trend. However, the balance predicted by Eq. (4) will only develop in the absence of other effects that influence nanodot size. As shown in Fig. 4(a), InAs undergoes an initial period of nucleation and growth that begins to saturate with increasing dose in a manner similar to GaAs and InP. However, the nanodots on InAs are prevented from ever reaching a stable size and distribution by the onset of a shape transition. The transition from pseudospherical nanodots at small sizes to faceted nanodots with increasing size is indicative of a surface energy driven transition.[38] The In nanodots on InP might be expected to undergo a similar transition if they were able to grow large enough. However, nanodots on InP reach a stable average size of ~33 nm and cease to increase in size beyond that point. Based on the assumptions above and the property values reported in Table IV, InAs and InP might be expected to have comparable In adatom surface diffusion rates and rates of sputtering losses from existing nanodots (as indicated by Y^*_{III}). However, the InAs rate of excess group III adatom production (Y_E) is twice as large as that of InP. The lower InP Y_E will result in slower nanodot growth in that system and following from Eqs. (4) and (5) will result in nanodots on InP being stabilized at a relatively smaller size. Correspondingly, the higher InAs Y_E allows nanodots on InAs to grow to larger sizes such that the system can reach the point where the bimodal transition occurs.

The balance of sputtering losses and nanodot growth predicted by Eq. (4) is insufficient to account for why AlAs does not form nanodots, but the property trends of Eq. (5) provide some insight. AlAs has small Y_E and D_{III} (as reflected by T_H) values, which indicate that relatively few adatoms will be generated from sputtering in the AlAs system and nanodot growth by diffusive processes will also be relatively slow. Al has a large γ value, indicating that Al nanodots will have a large energy barrier for nucleation. The combination of a high barrier to nanodot nucleation and expected low rate of growth by adatom attachment will act to prevent Al nanodots from forming on AlAs altogether or keep them from growing to a size above the detection limit of the instruments used in this work. This prediction is in agreement with the experimental observation that AlAs does not develop nanodots at room temperature even at high ion doses.

The large final average nanodot size in the GaAs case may be explained in a similar manner by examining the quantities of Eq. (5). GaAs has large Y_E and T_H values, indicating a large adatom production rate and high initial rate of diffusive growth. Ga also possesses a small Y^*_{III}, such that the rate of nanodot volume loss to sputtering will be slow. These effects collectively indicate that nanodots on GaAs will be able to grow to a larger average size before sputtering from them balances adatom addition and stabilizes the nanodot distribution. In contrast, InP has smaller Y_E and T_H values relative to GaAs and a large Y^*_{III} value. This indicates that nanodot growth by adatom diffusion will be slow in that system and that losses to sputtering will rapidly reach the point where they compensate nanodot growth. The smaller initial nanodots sizes of InAs may be similarly explained. InAs has a larger Y_E value than GaAs, but a smaller T_H value and larger Y^*_{III} value. Thus slower adatom diffusion and higher nanodot sputtering losses may still be keeping nanodot sizes in the InAs system (before its bimodal transition point) smaller than those of GaAs. The relative sizes of the

nanodots in the GaAs, InP, and InAs systems predicted by the trend of Eq. (5) agree with the experimental results reported earlier.

The qualitative trends visible in the above analysis reveal the basic physical phenomena controlling nanodot forming behavior. FIB response in the materials examined here is controlled both by those properties that determine their multicomponent sputtering behavior, and those that control the ability of group III adatoms to diffuse and collect into nanodots on the irradiated III-V surface. Both the multicomponent sputtering and adatom diffusion behavior of each compound can be related back to the relative strength of the atomic bonds holding atoms into the III-V structure or onto the III-V surface. Those materials with very high bond strength, like AlAs, are more resistant to sputtering and have more tightly bound surface atoms that diffuse slowly. As a result of this higher bond strength AlAs shows a lower rate of group III adatom production, a lower predicted adatom diffusion rate, and an observed difficulty in forming nanodots. In contrast, the lower atomic bond strength of InAs results in a high sputtering rate and excess group III adatom yield. The less tightly bound In surface atoms diffuse more quickly, resulting in a compound that forms nanodots readily under FIB irradiation. The relationship between atomic bond strength and the factors present in the models developed here to describe FIB response, such as Y_E, D_{III}, and Y^*_{III}, is clear. By consideration of the role of atomic bond strength and the resulting basic properties, the approach developed here may be used to better understand the FIB response of other multicomponent materials. The qualitative nature of the conclusions drawn above is necessitated by a lack of accurate values for many of the physical properties called for by the model of Eqs. (4) and (5). Further development of the model presented here and incorporation of a model for the nucleation kinetics of nanodots are needed to provide a more quantitative description of the III-V semiconductor FIB responses.

V. CONCLUSIONS

Despite belonging to the same class of compound semiconductor, GaAs, InP, InAs, and AlAs all have been shown to have different responses to focused Ga^+ ion irradiation. GaAs, InP, and InAs all form metallic group III nanodots following irradiation, but do so at different ion doses and develop different nanodot size distributions. At doses above $\sim 1.9 \times 10^{16}$ ions/cm^2 nanodots on InAs were observed to undergo a transition to a bimodal size distribution. No droplets were observed to form on AlAs. This work has made use of a model that combines sputtering theory and diffusive growth driven by Ostwald ripening to describe experimentally observed phenomena. The model predicts that for a system of growing nanodots, the competing effects of nanodot growth and losses due to sputtering will balance and result in a stable average nanodot size after an initial period of nanodot growth. Trends regarding the final stable nanodot size and the ease with which nanodots will nucleate and grow can be predicted using the physical quantities that make up the final form of the model. The experimentally observed Ga^+ FIB responses of each material examined agree qualitatively with the predictions of the model. Materials which have a higher rate of group III adatom diffusion across the irradiated semiconductor surface and a higher rate of excess group III atom production due to preferential sputtering will correspondingly have nanodots that are able to grow to larger sizes before growth is stopped by sputtering losses. In contrast, materials that exhibit a high pure group III sputtering yield and a high group III surface tension will have nanodots that are stabilized at smaller relative sizes. In keeping with classical nucleation theory, a high surface tension is also indicative of a high barrier to initial nanodot nucleation. All of these properties are in some capacity related to the relative atomic bonding strength of the III-V material or pure group III element. Those III-V compounds with higher bond strengths will sputter more slowly and have more tightly bound and slowly diffusing surface adatoms, resulting in smaller nanodots. Those that have weaker bond strengths will sputter more rapidly and produce more excess group III atoms. Stronger bonding in the group III nanodots will result in a lower sputtering rate from them and so stabilize larger nanodot sizes.

ACKNOWLEDGMENTS

This work was supported in part by the U.S. Army Research Office under Grant No. W911NF-07-1-0456.

APPENDIX

Following the general approach of Wei *et al.*,[11,32] a description for the growth of nanodots formed by ion irradiation of a compound material may be developed from the classic model for Ostwald ripening in a diffusion limited system[33] by adding an additional source term to account for adatom production by preferential sputtering. As a starting assumption, we take each metallic nanodot to be a spherical cap resting on an amorphous or otherwise ion disrupted III-V compound surface. The flux of excess group III adatoms diffusing to the nanodot may be found by solving the diffusion equation in polar coordinates for a radial area around each nanodot. Each spherical cap has a radius of curvature R and is surrounded by a denuded zone of radius λ, past which point the concentration of group III adatoms returns to the equilibrium concentration of a flat surface, C_0. The areal concentration of adatoms, $C(r,t)$, where r is the radial distance from the nanodot center and t is time, may be determined by solving

$$\frac{\partial C}{\partial t} = \frac{1}{r}\frac{\partial}{\partial r}\left[rD_{III}\frac{\partial C}{\partial r}\right] + Y_E I, \tag{A1}$$

where D_{III} is the diffusion coefficient of the excess group III atoms on the material surface. The second right-hand term takes into account the creation of excess group III atoms, and depends on the product of Y_E, the yield of excess group III atoms per ion, and I, the flux of incoming ions given in ions/cm^2/s. If steady state is reached such that diffusion of group III atoms to the nanodot is balanced by the addition of

adatoms into the capture volume enclosed by $R\sin(\theta) \leq r \leq \lambda$, where θ is the contact angle between the nanodot and III-V surface, then Eq. (A1) will have a solution of the form

$$C(r) = K_1 \ln(r) + K_2 - \frac{Y_E I r^2}{4D_{III}}, \tag{A2}$$

where K_1 and K_2 are constants. Let us assume now for the sake of simplicity that each nanodot is a hemispherical cap, such that $R\sin(\theta)=R$. This is a reasonable assumption, as Wei *et al.* found the wetting angle of Ga on GaAs to be near $\theta=90°$.[32] Experimental values of θ for the other compounds were not readily obtainable in this study due to the very small size of the In nanodots seen on InP and InAs and the absence of nanodots in the case of AlAs. The assumption that $\theta=90°$ allows the use of the boundary conditions

$$C(r) = C_R \quad \text{at} \quad r = R,$$

$$C(r) = C_\lambda \quad \text{at} \quad r = \lambda. \tag{A3}$$

Application of those conditions to Eq. (A2) results in

$$K_1 = \frac{(C_\lambda - C_R)}{\ln(\lambda/R)} + \frac{Y_E I}{4D_{III}} \frac{(\lambda^2 - R^2)}{\ln(\lambda/R)}. \tag{A4}$$

The number of group III atoms attaching per second to the periphery of the nanodot through surface diffusion is given by

$$J = 2\pi R \left[D \frac{\partial C}{\partial r} \right]_{r=R}. \tag{A5}$$

Substituting Eqs. (A2) and (A4) into Eq. (A5) produces

$$J = \frac{2\pi D_{III}(C_\lambda - C_R)}{\ln(\lambda/R)} + \pi Y_E I R^2 \left[\frac{(\lambda/R)^2 - 1}{\ln(\lambda/R)^2} - 1 \right]. \tag{A6}$$

The rate equation for change in hemispherical nanodot volume with time is

$$\frac{\partial}{\partial t}\left[\frac{2\pi R^3}{3}\right] = (J - 2\pi R^2 Y^*_{III} I)\Omega_{III} + \pi R^2 I \Omega_{Ga}, \tag{A7}$$

where Y^*_{III} is the sputtering yield of the pure group III element and Ω_{III} is the atomic volume of the group III atoms in a metallic nanodot, assumed to be approximately that of the bulk group III metal here. Ω_{Ga} is the atomic volume of Ga. The second term on the right side accounts for the loss of adatoms to FIB sputtering and the third term accounts for the addition of Ga atoms due to implantation in the nanodot by the FIB beam. Using the Gibbs–Thomson relationship, the equilibrium concentration, C_R, can be found by

$$C_R = C_0 + C_0 \left(\frac{2\Omega_{III}\gamma}{kT} \right) \frac{1}{R}, \tag{A8}$$

where γ is the metallic nanodot-vapor surface tension, k is the Boltzmann constant, and T is the absolute temperature. Substituting Eqs. (A6) and (A8) into Eq. (A7) produces

$$\frac{dR}{dt} = A\left(1 - \frac{R^*}{R} + BR^2\right), \tag{A9}$$

where

$$A(R) = \frac{D_{III}(C_\lambda - C_0)\Omega_{III}}{R^2 \ln(\lambda/R)},$$

$$R^* = \frac{2\Omega_{III}\gamma C_0}{kT(C_\lambda - C_0)},$$

$$B(R) = \left(\frac{Y_E I \ln(\lambda/R)}{2D_{III}(C_\lambda - C_0)} \right) \left[\frac{(\lambda/R)^2 - 1}{\ln(\lambda/R)^2} - 1 - 2\left(\frac{Y^*_{III}\Omega_{III} - 0.5\Omega_{Ga}}{Y_E \Omega_{III}} \right) \right]. \tag{A10}$$

This is the result arrived at by Wei *et al.*,[11,32] slightly altered to accommodate Y_E as defined in this paper and to generalize for the case of compounds beyond GaAs.

[1] M. Nisoli, S. Stagira, S. De Silvestri, A. Stella, P. Tognini, P. Cheyssac, and R. Kofman, Phys. Rev. Lett. **78**, 3575 (1997).
[2] P. C. Wu, A. S. Brown, M. Losurdo, G. Bruno, and H. D. Everitt, Appl. Phys. Lett. **90**, 103119 (2007).
[3] N. Koguchi and K. Ishige, Jpn. J. Appl. Phys., Part 1 **32**, 2052 (1993).
[4] K. Watanabe, N. Koguchi, and Y. Gotoh, Jpn. J. Appl. Phys., Part 2 **39**, L79 (2000).
[5] J. S. Kim and N. Koguchi, Appl. Phys. Lett. **85**, 5893 (2004).
[6] L. Hong, Z. Lui, X. T. Zhang, and S. K. Hark, Appl. Phys. Lett. **89**, 193105 (2006).
[7] A. Lugstein, B. Basnar, and E. Bertagnolli, J. Vac. Sci. Technol. B **20**, 2238 (2002).
[8] A. Lugstein, M. Weil, B. Basnar, C. Tomastik, and E. Bertagnolli, Nucl. Instrum. Methods Phys. Res. **222**, 91 (2004).
[9] A. Lugstein, B. Basnar, J. Smoliner, E. Bertagnolli, and M. Weil, J. Vac. Sci. Technol. B **22**, 2995 (2004).
[10] F. Rose, H. Fujita, and H. Kawakatsu, Nanotechnology **19**, 035301 (2008).
[11] Q. M. Wei, J. Lian, W. Lu, and L. M. Wang, Phys. Rev. Lett. **100**, 076103 (2008).
[12] A. Lugstein, B. Basnar, and E. Bertagnolli, J. Vac. Sci. Technol. B **22**, 888 (2004).
[13] V. Callegari and P. M. Nellen, Phys. Status Solidi., A Appl. Mater. Sci. **204**, 1665 (2007).
[14] A. Lugstein, B. Basnar, and E. Bertagnolli, Nucl. Instrum. Methods Phys. Res. B **217**, 402 (2004).
[15] J. H. Wu, W. Ye, B. L. Cardozo, D. Saltzman, K. Sun, H. Sun, J. F. Mansfield, and R. S. Goldman, Appl. Phys. Lett. **95**, 153107 (2009).
[16] A. Lugstein, J. Bernardi, C. Tomastik, and E. Bertagnolli, Appl. Phys. Lett. **88**, 163114 (2006).
[17] A. Lugstein, C. Schoendorfer, M. Weil, C. Tomastik, A. Jauss, and E. Bertagnolli, Nucl. Instrum. Methods Phys. Res. B **255**, 309 (2007).
[18] N. G. Chew and A. G. Cullis, Appl. Phys. Lett. **44**, 142 (1984).
[19] M. Nozu, M. Tanemura, and F. Okuyama, Surf. Sci. **304**, L468 (1994).
[20] S. K. Tan and A. T. S. Wee, J. Vac. Sci. Technol. B **24**, 1444 (2006).
[21] N. Nitta, M. Taniwaki, T. Suzuki, Y. Hayashi, Y. Satoh, and T. Yoshile, J. Jpn. Inst. Met. **64**, 1141 (2000).
[22] A. Perez-Bergquist, S. Zhu, K. Sun, X. Xiang, Y. Zhang, and L. M. Wang, Small **4**, 1119 (2008).
[23] K. S. Jones and C. J. Santana, J. Mater. Res. **6**, 1048 (1991).
[24] J. S. Williams, Mater. Sci. Eng., A **253**, 8 (1998).
[25] I. L. Singer, J. S. Murday, and L. R. Cooper, J. Vac. Sci. Technol. **18**, 161 (1981).
[26] P. Sigmund, in *Sputtering by Particle Bombardment I*, edited by R. Behrisch (Springer-Verlag, Berlin, 1981), Chap. 2.
[27] G. Betz and G. K. Wehner, in *Sputtering by Particle Bombardment II*, edited by R. Behrisch (Springer-Verlag, Berlin, 1983), Chap. 2.
[28] J. B. Malherbe and W. O. Barnard, Surf. Sci. **255**, 309 (1991).
[29] A. J. Moses, *The Practicing Scientist's Handbook* (Van Nostrand, New York, 1978), pp. 581–645.
[30] *CRC Handbook of Chemistry and Physics*, 89th ed., edited by D. R. Lide (CRC, Boca Raton, 2008), pp. 5–17.
[31] H. H. Anderson, in *Ion Implantation and Beam Processing*, edited by J. S. Williams and J. M. Poate (Academic, New York, 1984), Chap. 6.
[32] Q. M. Wei, Self-Organized Nanoscale Patterning under Ion Beam Irradia-

tion, PhD thesis, University of Michigan, 2009.
[33]B. K. Chakraverty, J. Phys. Chem. Solids **28**, 2413 (1967).
[34]B. K. Chakraverty, J. Phys. Chem. Solids **28**, 2401 (1967).
[35]V. K. Kumikov and Kh. B. Khokonov, J. Appl. Phys. **54**, 1346 (1983).
[36]http://www.srim.org/
[37]J. F. Ziegler, J. P. Biersack, and U. Littmark, *The Stopping and Range of Ions in Solids* (Pergamon, New York, 1985).
[38]A. W. Searcy, J. Solid State Chem. **48**, 93 (1983).